Mechanized deep tunnel excavation in saturated clayey soils: a pre-design hydro-mechanically coupled method for the assessment of both spoil and face volume loss

Author 1

● Luca Flessati

Faculty of Civil Engineering and Geoscience, Delft University of Technology, Delft, the Netherlands

Author 2

● Claudio di Prisco

Department of Civil and Environmental Engineering, Politecnico di Milano, Milan, Italy

Corresponding author

Luca Flessati

Faculty of Civil Engineering and Geoscience, Delft University of Technology, Delft, The Netherlands

Stevinweg 1, 2628 CN Delft the Netherlands

l.flessati@tudelft.nl

Abstract

Mechanized tunnel excavation in soils causes over-excavations, potentially leading to large amounts of spoil and settlements at ground level. An accurate estimation of over-excavations is crucial in the pre-design phase for assessing costs, determining the appropriate excavation method and choosing the muck management strategy. Currently, the estimation is based on experience and data from similar projects, but it becomes difficult when project conditions are heterogeneous. Alternatively, finite element analyses are time-consuming and not suitable for early design stages and, therefore, simplified tools are needed.

In this paper, the authors present a simplified approach putting in relation face extrusion with estimated spoil mass and face volume loss. This approach, conceived for deep tunnels, is the extension to the case of mechanized tunnelling of a hydro-mechanical coupled meta-model derived from finite element numerical analyses for tunnels in clayey soils excavated by using conventional techniques (i.e. without any use of tunnel boring machines).

The model has been validated against field data relative to a case study. The approach can be used in the early design process to identify tunnel boring machine characteristics and provide preliminary cost estimates. Additionally, during the construction phase, the method can be employed to interpret monitoring data and pre-design mitigation measures for unforeseen soil profile variations.

Keywords: face extrusion, spoil, face characteristic curve, volume loss, meta-model

1 Introduction

Excavating tunnels in soils may cause over-excavations, potentially resulting in large spoil masses and unexpected settlements at the ground level. An accurate estimation of the extent of over-excavation is crucial during the early design stages, such as planning and feasibility studies, as it allows: (i) the estimation of excavation costs and (ii) the selection of the most suitable excavation method and muck management strategy. Currently, the estimations of over-excavation is frequently based on experience and data gathered from similar projects, using the volume loss (the non-dimensional ratio of the volume per unit tunnel length of settlement trough at a given depth (usually at or near the surface) and the area of the excavated tunnel) as an indirect measure. However, when significant variations in project conditions are expected, the prediction of volume loss becomes very challenging without performing time-consuming non-linear finite element (FE) numerical analyses. Obviously, these analyses are not compatible with early design stages, where uncertainties regarding the mechanical behaviour of materials are unavoidable, and multiple potential solutions and mitigation strategies need to be considered. During early design phases, when preliminary cost has to be estimated and the most suitable excavation method is chosen, simplified tools must be employed.

As is suggested by many authors (Attewell & Farmer, 1974, Cording & Hansmire, 1975, Mair & Taylor, 1997, Vu et al., 2016), volume losses associated with mechanized tunnelling is usually calculated by adding four components: (i) volume loss at the tunnel face, (ii) volume loss along the shield, (iii) volume loss at the tail and (iv) long term volume loss due to consolidation. Among these four contributions, only the first one is related to the spoil mass. This is also associated with the face extrusion (i.e. the movement of soil toward the excavation chamber induced by the

62 variation in stresses in the advance core), therefore, its estimation requires the analysis of the
63 mechanical response of the face.
64 In the past, numerous authors have addressed this topic from various perspectives, including
65 theoretical, experimental, and numerical analyses.
66 In the literature, theoretical studies are mainly based on either the limit equilibrium method (Horn,
67 1961, Anagnostou & Kovari, 1996) or the limit analysis theory (Davis et al., 1980, Mühlhaus,
68 1985, Leca & Dormieux, 1990, Wong & Subrin, 2006, Klar et al., 2007, Mollon et al., 2009, 2013,
69 Pferdekämper & Anagnostou, 2022). Both the approaches allow the assessment of the minimum
70 pressure to prevent face collapse, but not face extrusion.
71 From an experimental point of view, both centrifuge (Mair, 1979, Kimura & Mair, 1981, Chambon
72 & Corté, 1994, Nomoto et al., 1999 Kamata & Mashimo, 2003) and 1g small scale model tests
73 (Sterpi & Cividini, 2004, Kirsch, 2009, Berthoz, 2012a, 2012b, Chen et al., 2013, Hu et al., 2022,
74 Shang et al, 2023) were performed to study the minimum pressure to be applied on the face to
75 ensure its stability. Therefore, these studies cannot be directly used to provide an estimation of face
76 extrusion. As far as 1g small scale model tests are concerned, particularly interesting are the results
77 in di Prisco et al. (2018b), in which the influence of the hydro-mechanical (HM) coupling on the
78 face response is discussed. The experimental results clearly put in evidence the fundamental role
79 of the excavation rate on face extrusion and, on the basis of the experimental results, a simplified
80 approach to estimate the minimum excavation rate, under which face mechanical response become
81 unstable, was proposed.
82 The importance of the role of HM coupling in affecting the face response was also numerically put
83 in evidence by many authors by performing FE numerical analyses (Callari, 2004, Callari &

84 Casini, 2006, Höfle et al., 2008, 2009, Callari, 2015 Sitarenios & Kavvadas, 2016, Callari et al.,
85 2017, Soe & Ukritchon, 2023).
86 FE numerical results have been also recently used to introduce “meta-models” (i.e. “upscaled
87 models” or “surrogate models”) suitable for deep tunnels excavated by means of conventional
88 tunnelling in saturated clayey soils (di Prisco et al., 2018a, di Prisco et al. 2019a, 2019b, di Prisco
89 et al. 2020, Flessati & di Prisco, 2022, Flessati & di Prisco, 2023). These meta-models are capable
90 of replicating FE results in relation to face extrusion and, once tunnel geometry and soil properties
91 are assigned, they can be employed to preliminarily calculate face extrusion without the need for
92 conducting FE simulations.
93 The objectives of this paper are:
94 (i) extending the meta-model introduced in di Prisco et al. (2019b) to the case of mechanized
95 tunnelling;
96 (ii) presenting a new simplified method putting in relation face extrusion and advancement rate for
97 tunnel excavated in saturated soils;
98 (iii) estimating both spoil mass and volume loss at tunnel face accounting hydro-mechanical
99 coupling for;
100 (iv) validate the method by comparing its blind predictions with field data.
101 This new method is a valuable tool to be used in the early design stages to preliminary estimate
102 both the costs associated with the spoil management and surface settlements. It is worth
103 mentioning this simplified approach is not intended to be used during the detailed and for-
104 construction design, when advanced FE simulations, reproducing in detail the tunnel boring
105 machine (TBM) subsystems are required. An exhaustive and recent discussion of this topic is
106 reported in Kratz et al. (2023).

For the sake of clarity, in Section 2 the meta-model introduced in di Prisco et al. (2019b) is briefly summarized. In Section 3 its extension to mechanized tunnelling is presented and finally, in Section 4, its practical application to a case study is illustrated.

2 Meta-model for the assessment of HM coupled face extrusion

The meta-model introduced in di Prisco et al. (2019b) is a relationship (named characteristic curve) between average face pressure (σ_f), excavation rate (v_{ex}) and average face extrusion (u_f). This does not imply that the stresses on the face and face displacement distributions are uniform. To conceive this meta-model and to train it, the results of a series of non-linear 3D FE numerical analyses were used. The assumptions of both HM coupled numerical analyses and meta-model are listed here below:

(i) the tunnel cross section is circular and the diameter is named D;

(ii) the cover diameter ratio (H/D) is assumed to be sufficiently large (H/D>4) to neglect the effect of the ground surface ("deep tunnel");

(iii) the water table is at the ground surface;

(iv) the tunnel is excavated in a saturated homogeneous soil layer characterized by a unit weight (γ_{sat}) constant along depth;

(v) the hydraulic behaviour is isotropic and permeability (k) is constant along depth;

(vi) the lining is rigid and impervious to water;

(vii) the excavation process is modelled as a progressive reduction in the pressure applied on the tunnel face and the time t_u to complete the face unloading is assumed to be coincident with the time necessary to excavate a tunnel length L_a=1.5D (L_a is the distance from the face from which stresses are practically not affected by the excavation, as is shown in di Prisco et al., 2022a), implying that $v_{ex}=1.5D/t_u$;

(viii) the soil behaviour is reproduced by using an elastic-perfectly plastic constitutive relationship with a Mohr-Coulomb failure criterion and a non-associated flow rule (nil dilatancy). In fact, when elastic-perfectly plastic constitutive relationship is employed to simulate the mechanical behaviour of a clay, the dilatancy at failure (that is at critical state) has to be nil.

Additional details regarding the numerical model are reported in Appendix 1.

For the sake of generality, the meta-model is defined by using the following non-dimensional variables:

$$Q_f = \frac{\sigma_{f0}-\sigma_f}{S_u^*} \qquad q_f = \frac{u_f}{u_{f,relu}}\frac{\sigma_{f0}}{S_u^*} \qquad \Upsilon = \frac{3(1-2\nu)\gamma_w D^2}{kEt_u}, \tag{1}$$

where σ_{f0} is the initial (geostatic) value of σ_f, γ_w is the water unit weight, ν is the Poisson ratio and E is the soil Young modulus, assumed to be constant in the soil domain. S_u^* is a strength parameter depending on the boundary value problem accounted for and can be written as: $S_u^* = \alpha S_{u,e}$. α only depends on friction angle ϕ' (Appendix 2). $S_{u,e}$ is the value of the soil undrained strength calculated (by adopting the constitutive relationship used for the FE simulations) by imposing the geostatic effective pressure at tunnel axis depth (p^*) and an undrained extension stress path ($S_{u,e} = M_e/2 \cdot p^*$, being $M_e = 6sin\phi'/(3+sin\phi')$). $u_{f,relu}$ represents the undrained elastic residual (i.e. for σ_f=0) face extrusion (di Prisco et al., 2018a):

$$u_{f,relu} = \frac{2}{3}\frac{1+\nu}{K_{el}}\frac{\sigma_{f0}}{E}D, \tag{2}$$

where K_{el} is a non-dimensional parameter depending on the H/D value. The numerical FE results reported in di Prisco et al. (2018a) allow to conclude that for H/D>5 K_{el} is practically constant and equal to 3.

The non-dimensional definitions of variables Q_f and q_f come from the analytical solution of undrained tunnel cavities in unbounded media (di Prisco et al., 2018a), whereas the non-dimensional definition of ϒ comes from the equation of mass balance of water (Appendix 3). The definition of the meta-model in terms of non-dimensional variables makes the meta-model reliable for any geometry/soil property value, extending infinitely its range of applicability.

According to di Prisco et al. (2019b), the use of these non-dimensional variables is particularly convenient since, for any given value of ϒ, a unique global (characteristic curve) and local (stress, pore pressure, strains and displacement fields) response, independent of both geometry and soil hydraulic/mechanical properties, is obtained (Appendix 4).

According to the meta-model, the relation between Q_f and q_f can be expressed as it follows:

$$q_f(Q_f,\Upsilon)=\begin{cases}\dfrac{Q_f}{R(\Upsilon)}, & Q_f<a_f(\Upsilon)\\ \dfrac{a_f(\Upsilon)}{R(\Upsilon)}e^{\frac{Q_f}{a_f(\Upsilon)}}+\dfrac{Q_f-a_f(\Upsilon)}{Q_L(\Upsilon)-Q_f}, & Q_f>a_f(\Upsilon)\end{cases} \tag{3}$$

where $R(\Upsilon)$, $a_f(\Upsilon)$ and $Q_L(\Upsilon)$ are functions governing respectively: the initial inclination of the characteristic curves, transition from the initial linear to the non-linear response and the limit/collapse value for Q_f. The training of the model consisted in using FE results to define the functions $R(\Upsilon)$, $a_f(\Upsilon)$ and $Q_L(\Upsilon)$ (Appendix 5).

The characteristic curves obtained by using this meta-model (solid and dashed lines) are compared in Figure 1 with FE numerical results (symbols). Geometry and soil properties employed to obtain the numerical results are reported in Table 1. In these cases, the at rest lateral earth pressure (k_0) is assumed to be equal to one and different v_{ex} were considered. An extension to different k_0 values

is quite simple and implies only a change in one meta-model parameter (a_{fu} defined in Appendix 5). As is evident in Figure 1 the meta-model can satisfactorily reproduce FE results for any value.

Table 1: Geometry and soil mechanical/hydraulic properties

D [m]	H/D [-]	E [MPa]	ν [-]	c' [kPa]	ϕ' [°]	ψ [°]	γ_{sat} [kN/m^3]	k [m/s]
15	7	85	0.3	0	25	0	20	10^{-9}

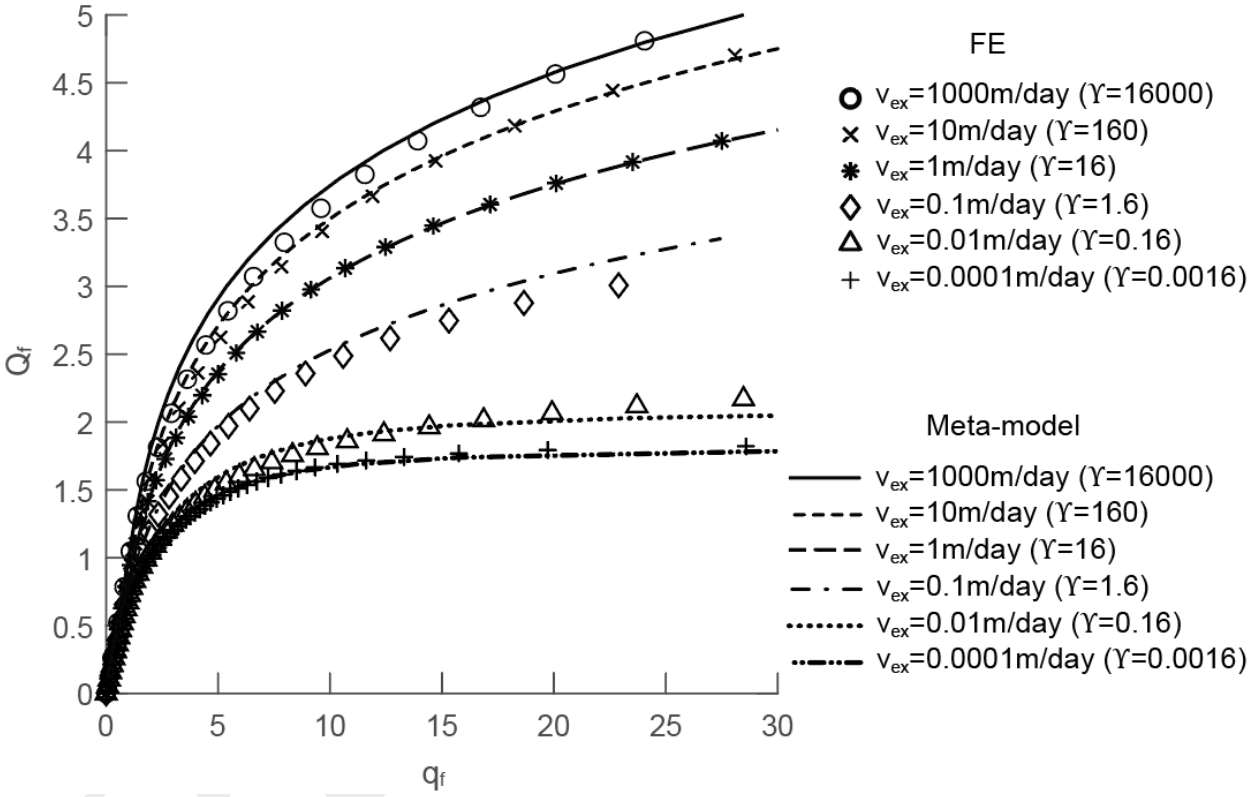

Figure 1: non-dimensional face characteristic curves

Despite the simplicity of the constitutive relationship adopted, the numerical results capture very satisfactory the mechanical processes taking place in the soil domain. This is testified by the slight dependence of non-dimensional face characteristic curves on the constitutive relationship implemented in the numerical code. In Flessati & di Prisco (2018) the authors illustrated the non-

dimensional characteristic curves obtained by implementing the Modified Cam Clay model and have shown that the correct assessment of S_u^* allows to obtain curves practically coincident with those obtained by using an elastic-perfectly plastic constitutive relationship.

In di Prisco et al. (2019b) the meta-model is also validated by using the results of a series of 1g small scale model experimental tests (tests A1-A4 of di Prisco et al., 2018b). The hydro/mechanical properties of the soil employed correspond to those of the material employed for the small scale tests (Flessati, 2017). In Figure 2, the residual displacements ($u_{f,r}$) are illustrated versus v_{ex}. Again, the agreement is satisfactory.

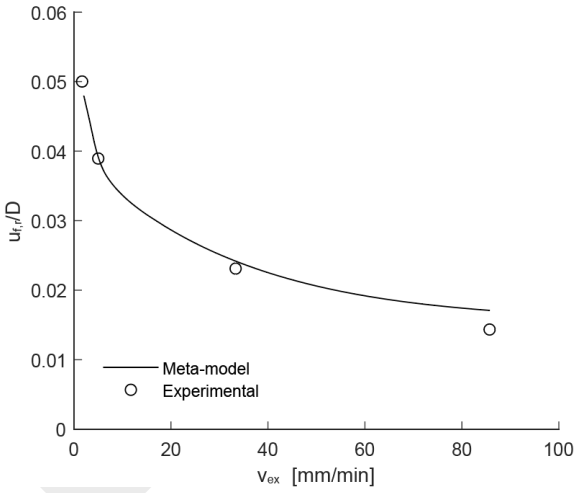

Figure 2: Comparison between blind predictions with the meta-model and experimental results (adapted from di Prisco et al, 2018b)

An alternative representation of Equation 3 is provided in Figure 3a, where iso-q_f curves are plotted. All these curves are characterized by two horizontal branches, one for small ($\Upsilon < 10^{-1}$) and one for large ($\Upsilon > 10^{4}$) Υ values, corresponding, respectively, to drained and undrained face responses. All the other Υ values ($10^{-1} < \Upsilon < 10^{4}$) identify "partially drained" face responses. In this Υ range, the face response is significantly affected by Υ (in particular in the interval $1 < \Upsilon < 10$), implying that

increases/reductions in the excavation rate may significantly decrease/increase face extrusion. Figure 3a is a very useful tool in the early phases of the pre-design stage, since it allows, with a negligible computational effort (only the definition of both geometry/soil properties and the calculation of the non-dimensional variables are required), to estimate the face displacements associated with an assigned excavation rate.

It is worth mentioning that, in case of deep tunnels, for large excavation rates (undrained response), the system is not characterized by the development of a failure mechanism (as is observed in di Prisco et al. (2018a) the stiffness of the characteristic curve never nullifies) although the extrusion values may be unacceptable. In other words, from a mechanical point of view, the knowledge of a face extrusion value (or equivalently of volume loss at the tunnel face) does not provide a priori hints on the stability of the face. To clarify this concept, in Figure 3b the variation in the characteristic curve stiffness (dQ_f/dq_f) with Υ is plotted. Each curve corresponds to a different q_f value. As is expected, for all the q_f values, a decrease in Υ is associated with a reduction in stiffness. For large q_f values (q_f>20) a very pronounced reduction in stiffness is evident for $\Upsilon < 5$. This implies that for $\Upsilon < 5$ the face may be at failure.

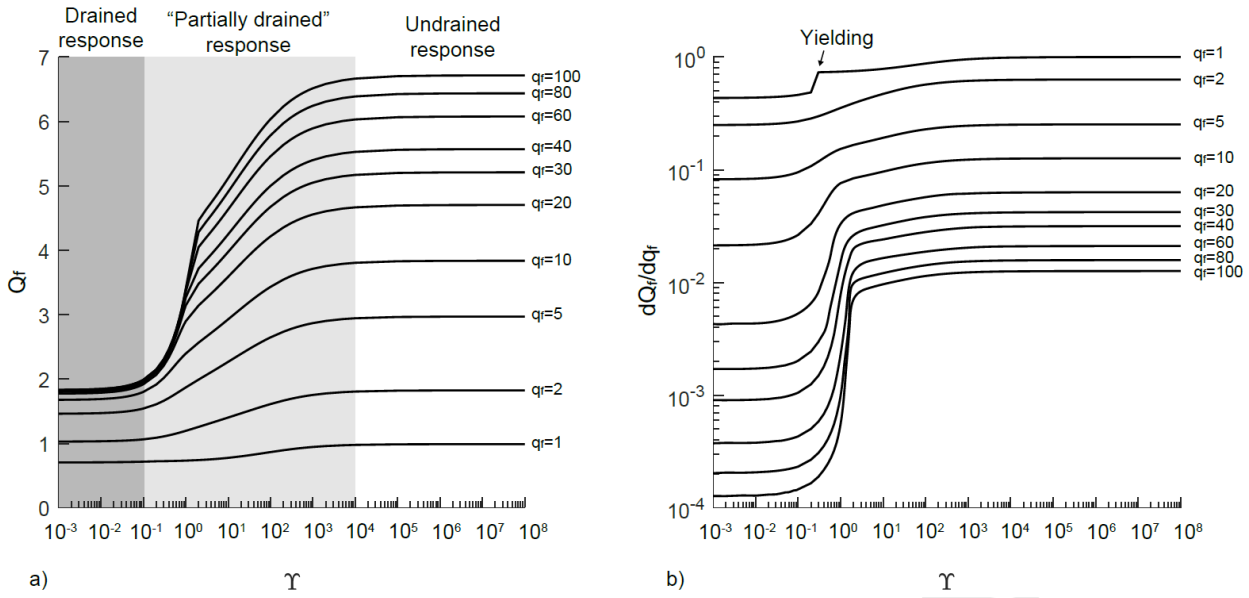

Figure 3: Tunnel face characteristic curves: a) in the Qf - ϒ plane and b) in the dQf /dqf – ϒ plane

3 Application to the case of mechanized tunnelling

As was previously mentioned, the meta-model briefly outlined in the previous section was originally conceived for conventional tunnelling, that is for unsupported faces for which extrusion (q_f=q_{fus}, *us* stands for unsupported, Figure 4) is calculated by imposing in Equation 3 σ_f=0 and:

$$Q_f = Q_{fus} = \frac{\sigma_{f0}}{s_u^*}. \quad (4)$$

In contrast, in case of mechanized tunnelling, face extrusion (q_f=q_{fs}, *s* stands for supported, Figure 4) has to be calculated by imposing:

$$Q_f = Q_{fs} = \frac{\sigma_{f0}-\sigma_{f,TBM}}{s_u^*} = Q_{fus} - Q_{TBM}, \quad (5)$$

where $\sigma_{f,TBM}$ is the pressure applied on the tunnel face by the TBM head. As is expected, the larger the TBM face pressure, the smaller is the face extrusion (Figure 4).

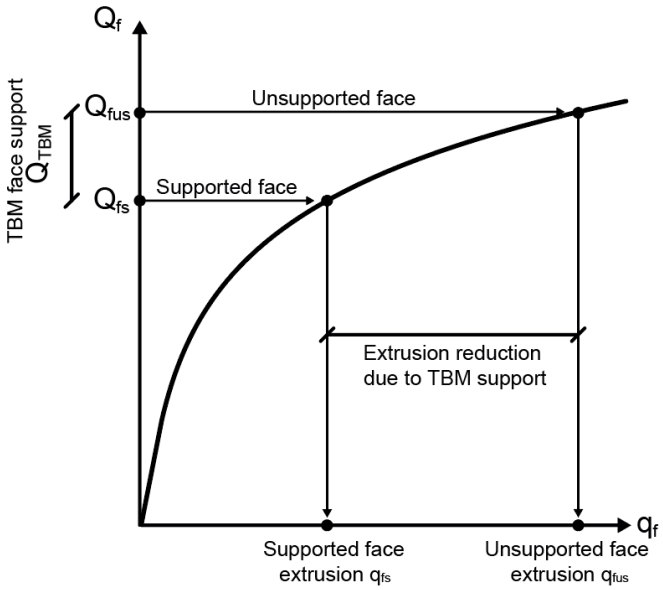

Figure 4: Face extrusion reduction due to TBM face pressure

As was previously mentioned, from a design standpoint, the meta-model offers the advantage of providing an initial assessment of face extrusion without the need of performing any FE numerical simulations. In the subsequent sections, the extrusion value will be used, by following a novel procedure, to estimate spoil mass and volume loss at tunnel face, accounting the hydro-mechanical coupling for. Moreover, apart from this direct application, the meta-model can also be employed in the preliminary design phase for two additional purposes: (i) determining whether face support is necessary and (ii) selecting $\sigma_{f,TBM}$ based on a displacement-based design approach (Figure 5). In this case the meta-model is used as it follows:

1. Υ and Q_{fus} are calculated by means of Equations 1 and 4, respectively;

2. the value of the unsupported face extrusion (q_{fus}) is calculated by introducing Υ and Q_{fus} in Equation 3;
3. a value of admissible face extrusion $u_{f,adm}$ is assigned (e.g. from limitations on the maximum admissible volume loss) and by using Equation 1 the corresponding non-dimensional value ($q_{f,adm}$) is calculated;
4. if $q_{fus}<q_{f,adm}$ face support is not required, whereas if $q_{fus}>q_{f,adm}$ face support is required. In this second case, Q_{fs} is calculated by imposing $q_f=q_{f,adm}$ in Equation 3 and finally and $\sigma_{f,TBM}$ is calculated by using Equation 5.

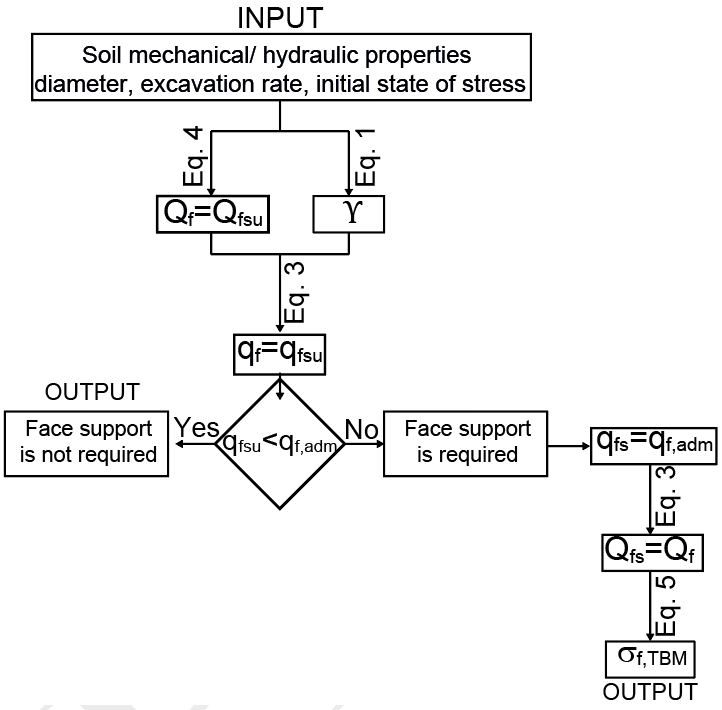

Figure 5: Design of TBM face pressure

Even during the excavation, the meta-model is very useful since it allows (i) alongside monitoring data, to confirm the design assumptions related to soil hydraulic and mechanical properties and (ii) to choose potential countermeasures such as either adjusting face pressure or advance rate in response to unforeseen and inevitable soil profile changes.

3.1 Spoil weight assessment

As a first approximation, the spoil weight extracted for each segmental lining ring (W_s) can be calculated by summing a term W_r, related to the volume of the ideal excavation cross section of length L_r (the lining segment length) and a term W_e varying with advance rate and face pressure, related to u_f:

$$W_s = W_r + W_e = \frac{\gamma_{sat}\pi D^2}{4} L_r + \frac{\gamma_{sat}\pi D^2}{4} u_f \quad (6)$$

The dependence of W_s on both $\sigma_{f,TBM}$ and v_{ex} is illustrated in Figure 6, for L_r=*2m* and for geometry and soil properties of Table 1. The four lines represented in Figure 6a are obtained by imposing v_{ex}=1, 2, 5 and 10m/day, whereas the two lines of Figure 6b by imposing $\sigma_{f,TBM}$ = 180 and 360kPa. As was expected, for a fixed value of v_{ex}, a reduction in $\sigma_{f,TBM}$ implies an increase in W_s (Figure 6a). The minimum W_s value (W_s=W_r) corresponds to the (ideal) case $\sigma_{f,TBM}$=σ_{f0}, for which overexcavation is nil (u_f=0).

The results of Figure 6b highlight that, as was expected, W_s decreases by increasing the excavation rate. Nevertheless, for the case considered (D=15m, k=10^{-9} m/s and E=85MPa) this reduction is practically negligible for v_{ex}>10 m/day, since for v_{ex}>10 m/day the system response is practically undrained. However, this result is not general and strictly dependent on both soil permeability and tunnel diameter (Equation 3).

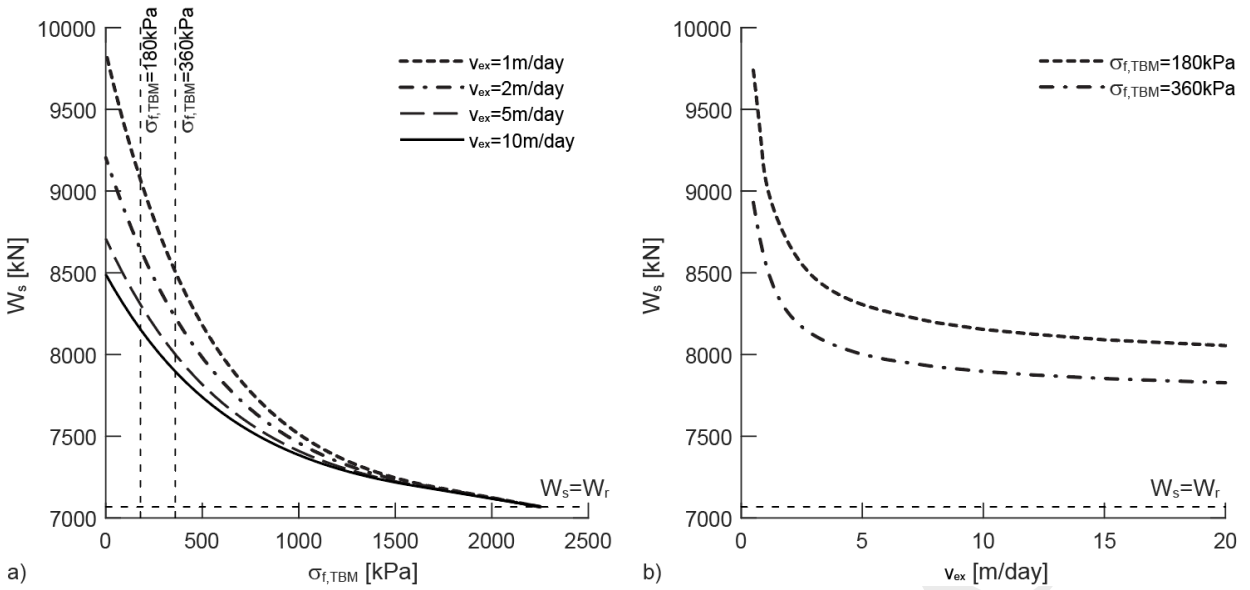

Figure 6: Variation of W_s with (a) TBM face pressure (v_{ex}=1÷10m/day) and (b) excavation rate ($\sigma_{f,TBM}$=180, 360kPa)

3.2 At face volume loss assessment

Under the assumption that the tunnel face effect propagates for a length L_a (di Prisco et al, 2022a), we can write that:

$$V_{L,f} = \frac{u_f}{L_a} \tag{7}$$

where $V_{L,f}$ is the volume loss at the face.

In Figure 7 the dependence of $V_{L,f}$ with both $\sigma_{f,TBM}$ and v_{ex} is illustrated for the reference case (Table 1). The four curves of Figure 7a refer to v_{ex} =1, 2, 5 and 10m/day, whereas the results of Figure 7b to two values of $\sigma_{f,TBM}$ (180 and 360kPa).

As was expected, a reduction in $\sigma_{f,TBM}$ implies an increase in $V_{L,f}$ (Figure 7a) and the minimum value of zero corresponds to the ideal case $\sigma_{f,TBM}$=σ_{f0}, for which u_f=0.

$V_{L,f}$ decreases by increasing the excavation rate. Nevertheless, for the case considered (D=15m, k=10^{-9} m/s and E=85MPa) this reduction is practically negligible for v_{ex}>10 m/day, but this result is not general since it depends on soil permeability and tunnel diameter (Equation 3).

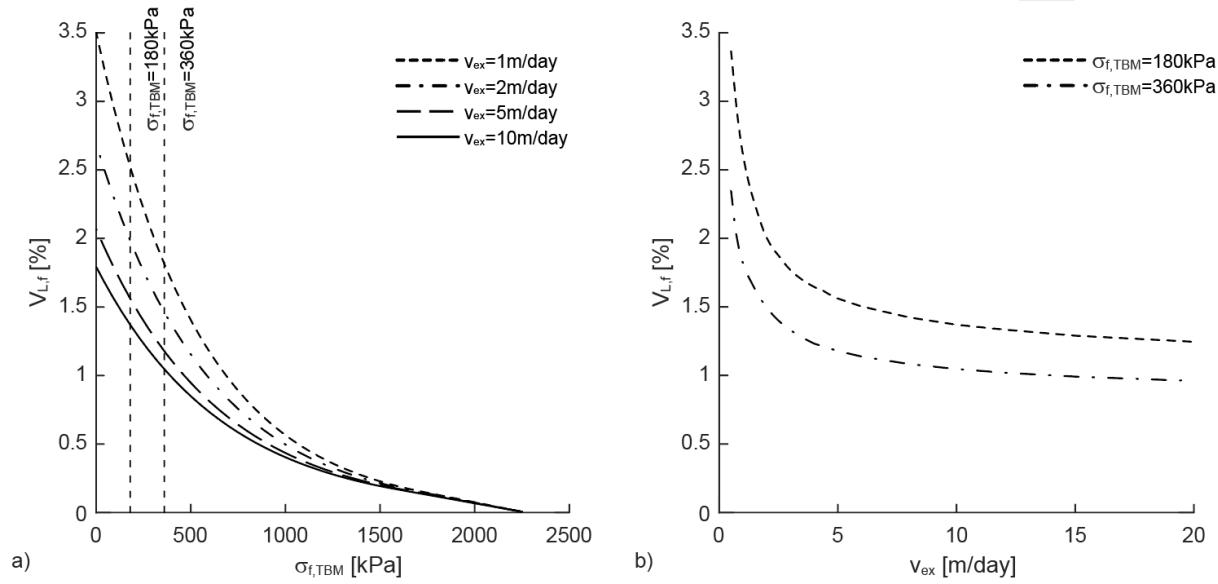

Figure 7:Variation of $V_{L,f}$ with (a) TBM face pressure (v_{ex}=1÷10m/day) and (b) excavation rate ($\sigma_{f,TBM}$=180, 360kPa)

It is worth mentioning that the method here proposed, conversely to the empirical expressions and simplified formulas commonly employed (Clough & Schmidt, 1981, Attewell et al., 1986, Mitchell, 1983, Macklin, 1999), explicitly takes three key factors into consideration: (i) the tunnel geometry (in terms of diameter and depth), (ii) mechanical and hydraulic soil properties, and (iii) TBM excavation parameters (excavation rate and face pressure).

4. Application to a case study

The ground surface profile and the water table level relative to the case study are sketched in Figure 8a. An enlargement of the area of interest for this paper is reported in Figure 8b. The stratigraphy

is characterized by four geological formations, but, the laboratory test results obtained in the for-construction design stage highlighted that, from a mechanical point of view, the behaviour of the three deeper layers is coincident and therefore the tunnel is assumed to be excavated in a unique homogeneous normally-consolidated clayey soil layer (Table 2).

Table 2: Soil mechanical/hydraulic properties (derived from for-construction design)

	Unit weight [kN/m^3]	Young modulus [MPa]	Poisson ratio [-]	Cohesion [kPa]	Friction angle [°]	Dilatancy angle [°]	Permeability [m/s]
Clays & silty clays	22.3	85	0.3	5	23	0	10^{-9}
Argillaceous marls	22.3	85	0.3	0	25	0	10^{-9}
Calcareous marls	22.3	85	0.3	0	25	0	10^{-9}
Limey marls	22.3	85	0.3	0	25	0	10^{-9}

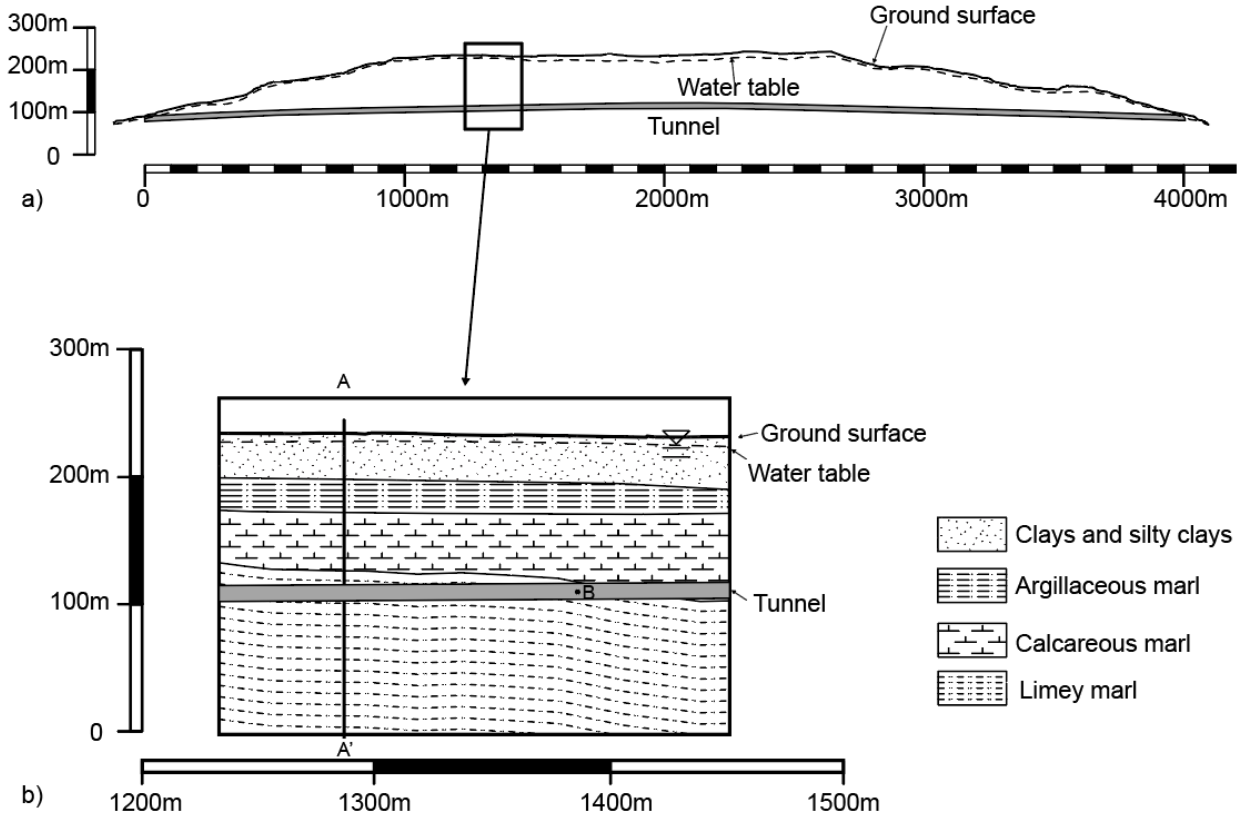

Figure 8: (a) sketch of the ground surface and (b) detail of the geological formations in the area of interest

326 The tunnel was excavated by means of an Earth Pressure Balance-TBM. The TBM head diameter
327 was 15.08m and the average overcut (δ) was 0.045m. The length of the shield was 12.8m. The
328 segmental lining was characterized by a thickness of 60 cm and the ring was 2m long. The
329 backfilling was realized by using a two-component grout (water/bentonite mass ratio 20/1,
330 cement/bentonite mass ratio 8/1) injected at a pressure 50kPa larger than face pressure. The spoil
331 was extracted by means of a belt conveyor, allowing to directly measure the spoil weight (soil +
332 conditioning).
333 During the excavation process, the vertical displacements of the ground surface were monitored at
334 cross section A-A' (of Figure 8b). Measured settlements at the ground level are illustrated in Figure
335 9. Specifically, the maximum measured displacement is related with the distance from the tunnel
336 face in Figure 9a, whereas in Figure 9b it is related with time. In Figure 9c the final spatial
337 settlement distribution is plotted (circle symbols).
338

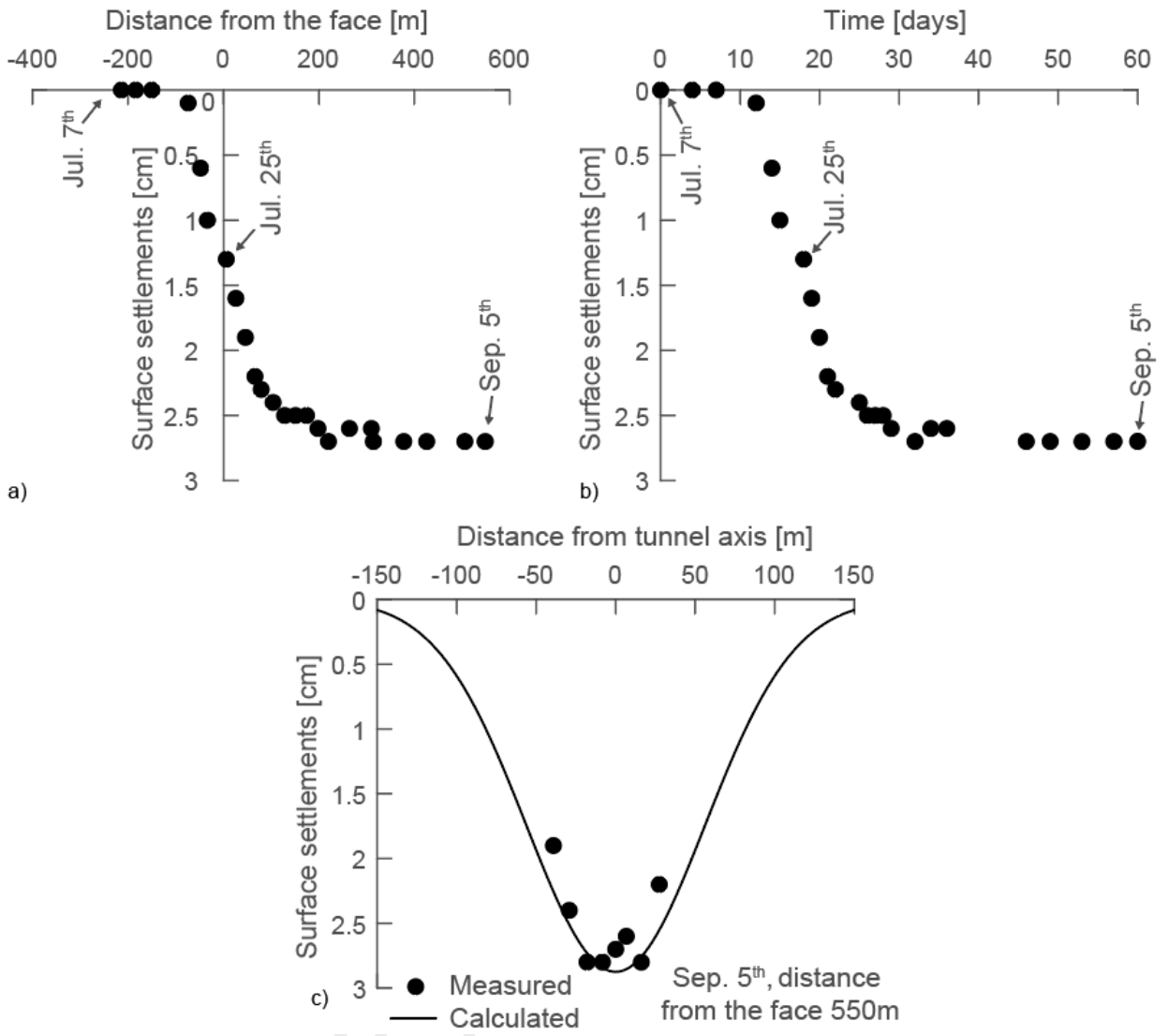

Figure 9: Surface settlement measures in section A of Figure 8b: (a) evolution with distance of the face along the tunnel axis, (b) evolution with time along the tunnel axis and (c) final values perpendicular to the tunnel axis

Furthermore, owing to the presence of a parallel tunnel, a horizontal inclinometer was installed at point B (Figure 8b) perpendicularly to the excavated tunnel axis (Figure 10a and 10b). This setup allowed the designers to measure the progressive evolution of horizontal displacements caused by the tunnel face approaching. The measured values corresponding to different values of face distance are plotted in Figure 10c, whereas the evolution of the average values in the excavated tunnel cross section (circles) in Figure 10d.

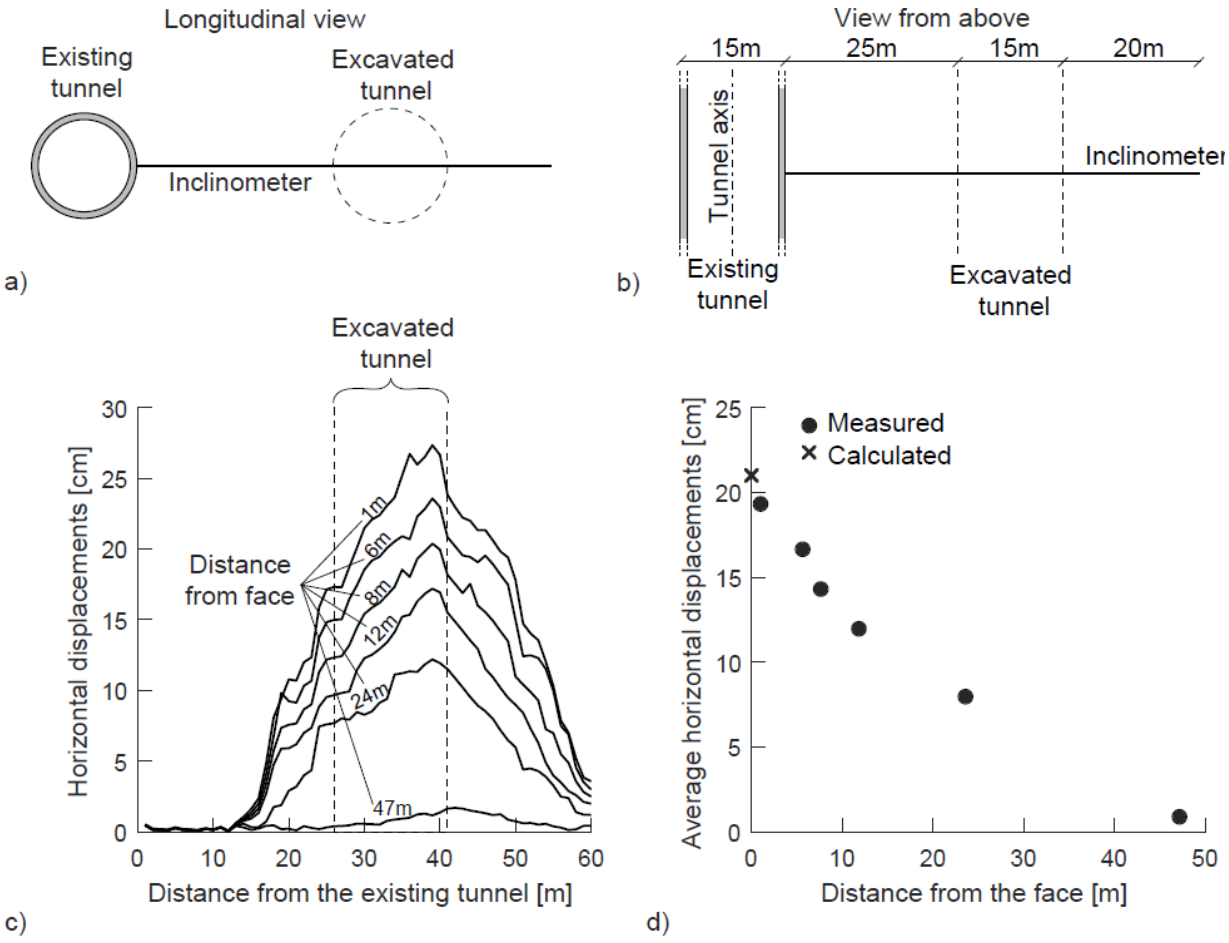

Figure 10: (a) and (b) horizontal inclinometer installed from an existing tunnel (longitudinal view and view from above, respectively), (c) horizontal displacements measured at different distance from the face and (d) average values of horizontal displacements in the tunnel cross section

In the considered area of interest (Figure 8b) both ground surface and water table level are almost horizontal. The tunnel cover is equal to 112m ($H/D \cong 7.5$) and the water table level is located at a depth of 20m from the ground surface.

To apply the simplified approach described in Sections 2 and 3, the following assumptions were introduced:

- the soil mechanical/hydraulic properties and the at rest lateral earth pressure coefficient (k_0=1) were derived from the for-construction design (values of Table 2 relative to limey marls);
- the values of TBM advancement rate (v_{ex}=13.5m/day) and face pressure ($\sigma_{f,TBM}$=360kPa) are the average values measured during the excavation;
- the limit value of the average horizontal displacement in the cross section (Figure 10d) for a zero distance from the face is identified as the face extrusion.

For this reason, all the results of the simplified approach have to be interpreted as a "blind prediction" since none of the input data was back analysed.

As was previously mentioned, the practical use of the approach introduced by the authors requires the definition of input data such as geometry, soil mechanical/hydraulic properties and TBM excavation parameters and the use of the equations reported in Sections 2, 3 and in Appendix 5. For the sake of clarity, a flow chart illustrating the practical employment of the approach is reported in Figure 11. The predicted face extrusion value of 21cm (cross symbol in Figure 10d) is in very good agreement with the average values of displacements measured by the inclinometer.

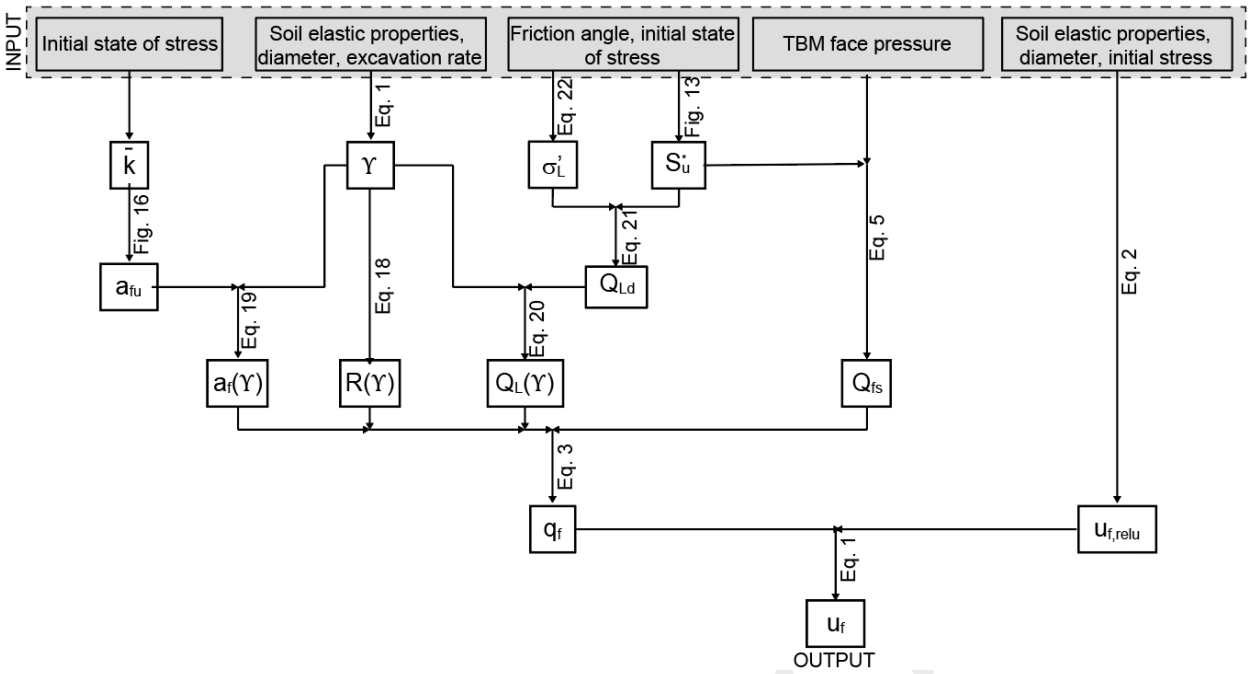

Figure 11: Flowchart of the simplified design approach for calculating face extrusion

The average weight of the extracted soil (excluding the conditioning weight) for each ring length (2m), measured along the tunnel excavation, was equal to 9120kN. By introducing the calculated value of face extrusion (21cm) into Equation 6, W_s=8950kN. Again, the agreement is very satisfactory (the error in the prediction is lower than 4%).

The surface settlement profile at the ground surface (S) is calculated by following the standard approach proposed in Peck (1969) according to which:

$$S = \frac{0.31 V_L}{i} D^2 \exp\left(-\frac{x^2}{2i^2}\right), \quad (8)$$

where V_L is volume loss, x is the horizontal coordinate perpendicular to the tunnel axis and starting from the tunnel centre and

$$i = k^* \left(H + \frac{D}{2}\right), \quad (9)$$

where k^* is an empirical coefficient depending on the type of soil (Mair & Taylor, 1997, di Prisco et al., 2022b).

As was previously mentioned, V_L is assumed to be given by the sum of four volume loss contributions: volume loss at the tunnel face, volume loss along the shield ($V_{L,s}$), volume loss at the tail ($V_{L,t}$) and long term volume loss due to consolidation ($V_{L,l}$).

The volume loss at the face ($V_{L,f}$*=0.9%*) is assessed by using Equation 7 in which the calculated value of face extrusion (21 cm) was introduced.

Since the face pressure is significantly lower than geostatic vertical stresses, the soil is assumed to be moving toward the cavity associated with the TBM conicity (Vu et al., 2016). By following the approach proposed in Dimmock & Mair (2007):

$$V_{L,S} = \frac{4\delta}{D} = 1.2\% \quad (10)$$

By following what was suggested in Vu et al. (2016), the volume loss at the tail can be calculated by using the cavity expansion theory. The maximum value of settlement calculated by using this theory and by using the average value of back filling injection pressure (360+50kPa) is equal to 0.8mm. Since this value is practically negligible with respect to the measured maximum displacement values (approximately equal to 3cm, as is shown in Figure 9c), the authors assumed $V_{L,t} = 0$.

The evolution of ground surface settlements with time (Figure 9b) is characterized by an almost constant trend for large time values, highlighting (in the period considered by the monitoring

414 system) a negligible role of the consolidation process on settlements. For this reason, the authors
415 assume $V_{L,l}$=0.
416 The gaussian curve reproducing the ground surface settlements obtained by assuming $V_L = V_{L,f} +$
417 $V_{L,s}$=2.1% and k^*=0.47 is plotted in Figure 9c (solid line). k^* was fitted on the experimental
418 measures to capture the amplitude of the settlement through. The value of k^* is in agreement with
419 the values suggested in Mair & Taylor (1997) for clayey materials (ranging in between 0.4 and
420 0.6). As is evident in Figure 9c, the calculated settlement profile is almost coincident with the
421 measured one (the maximum absolute error is approximately equal to 2mm).
422 In the literature simplified methods, estimating volume loss dependence on excavation rate in
423 saturated clayey soils, are not available. According to Macklin (1999), in the case here above,
424 V_L=0.88% and, by means of Equation 8, the maximum settlement would be 1.1 cm, a value
425 significantly smaller than the one measured (Figure 9).
426
427 **5. Concluding remarks**
428 In this paper an approach developed to estimate face extrusion in conventional tunnelling is
429 extended to the case of mechanized tunnelling. The proposed approach is applicable to deep
430 tunnels excavated in saturated clayey materials and is based on a meta-model accounting hydro-
431 mechanical coupling for. By employing the novel method introduced in this paper, the calculated
432 values of face extrusion are used to estimate spoil weight and volume loss at tunnel face.
433 The model predictions were compared to measurements from a case study, and the agreement was
434 highly satisfactory. From a practical perspective, the approach introduced by the authors can be
435 employed during the early stages of the design process for the following purposes: (i) identifying
436 the required characteristics of the tunnel boring machine, such as maximum face pressure and

437 excavation rate, when admissible surface settlements are defined, and (ii) providing preliminary
438 cost estimates for construction.
439 Furthermore, during the construction phase, this method is useful in (i) critically interpreting
440 monitoring data and (ii) pre-designing suitable mitigation measures (e.g. variation in face pressure
441 or in the excavation rate), if necessary, in cases of unforeseen or unavoidable variations in the soil
442 profile.
443 The meta-model equations are implemented in a code available in
444 https://github.com/LFlessati/TunnelFace
445
446 **Appendix 1**
447 The meta-model was conceived by interpreting the numerical results obtained by performing a
448 series of 3D hydro-mechanical coupled FE numerical analyses, considering a circular tunnel of
449 diameter D excavated in a homogeneous clayey soil layer (Figure 12a). The tunnel cover diameter
450 ratio (*H/D*) is assumed to be sufficiently large (greater or equal to 4) to neglect the effects of the
451 ground surface ("deep tunnel"). The saturated soil unit weight is assumed be constant along depth
452 and permeability to be isotropic and constant along depth. The lining is assumed to be rigid.
453 The soil mechanical behaviour is assumed to be elastic-perfectly plastic. The elastic properties,
454 Young modulus and Poisson ratio are assumed to be constant along depth. The yield surface is
455 defined by the Mohr-Coulomb criterion and the flow rule to be non-associated. Despite its
456 simplicity, this constitutive relationship can capture the main aspects of the mechanical processes
457 taking place in the soil domain. The use of more sophisticated constitutive laws (such as strain
458 hardening elastic plastic constitutive relationships) confirms this statement (Flessati & di Prisco,
459 2018).

On the lower and lateral boundaries of the domain normal displacements are imposed to be zero. The water table level is assumed to be coincident with the ground surface and all the other boundaries are assumed to be impervious to water.

In analogy to what was done in Chambon & Corté, 1994, Vermeer et al., (2003), Sterpi & Cividini, 2004, Kirsch, 2009, di Prisco et al., 2018a, 2018b, di Prisco et al., 2020 the excavation process is modelled as a progressive reduction in the pressure applied at the face (Figure 12b).

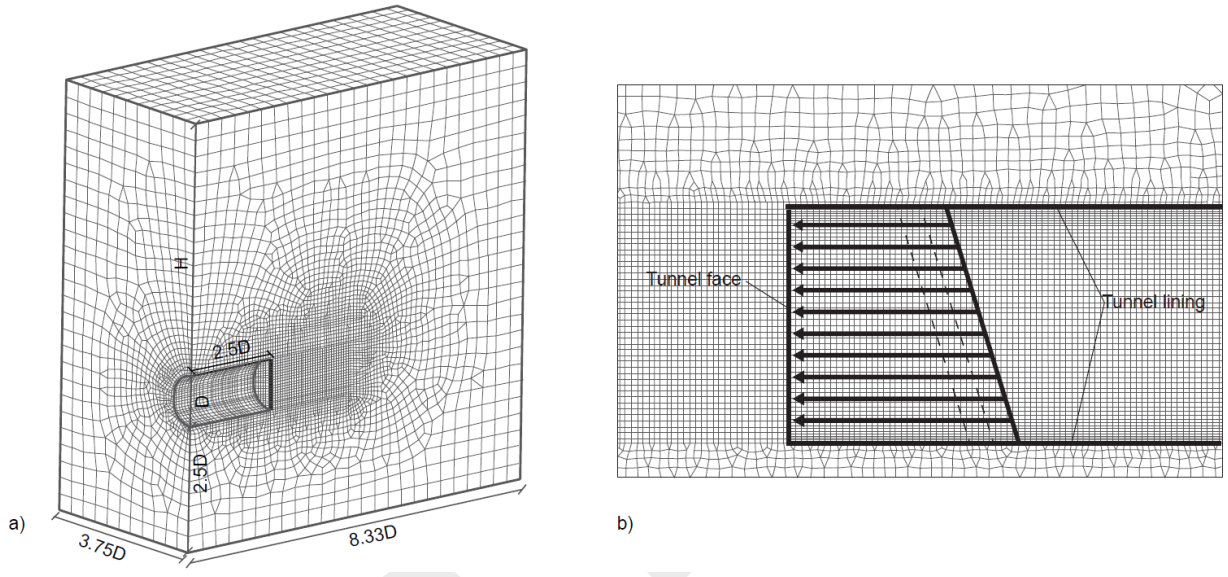

Figure 12: (a) numerical model and (b) progressive reduction in pressure applied at the face (adapted from di Prisco et al., 2018a)

Appendix 2

The FE numerical results (di Prisco et al., 2019b) employed to introduce the meta-model were obtained by implementing a Mohr-Coulomb failure criterion and by performing hydro-mechanical coupled numerical analyses. This implies that, when rapid excavation processes are simulated (undrained conditions), different undrained strength (S_u) values are locally obtained according to the stress paths followed by each point belonging to the spatial domain.

As was previously mentioned, $S_u^* = \alpha\, S_{u,e}$ and the authors observed that α is only a function of ϕ' Figure 13. Figure 13 allows to calculate α and therefore S_u^* once both the internal friction angle and tunnel axis depth are assigned.

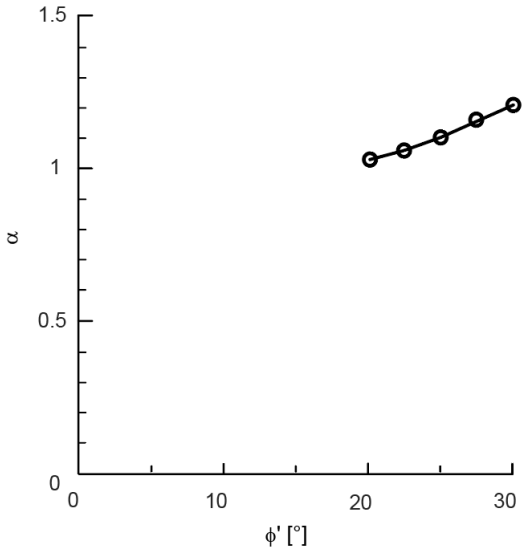

Figure 13 Variation of α with ϕ'

Appendix 3

The influence of the excavation rate on the system response is related to excess pore water pressure dissipation. This is governed by the water mass balance equation:

$$k\left(\frac{\partial^2 h}{\partial x_1^2}+\frac{\partial^2 h}{\partial x_2^2}+\frac{\partial^2 h}{\partial x_3^2}\right)=-\frac{\partial\, \varepsilon_{vol}}{\partial t}, \qquad (11)$$

where h is the hydraulic head, ε_{vol} the volumetric strain and x_1, x_2 and x_3 define a coordinate system (hydraulic conductivity is assumed to be constant and the material to be hydraulically isotropic). In case the material behaviour is assumed to obey to an isotropic elastic-plastic constitutive relationship with no dilatancy:

$$\varepsilon_{vol} = \frac{p'}{K} = \frac{p - u^e - u^s}{K}, \quad (12)$$

where p' and p are the effective and total pressure, u^e is the excess pore water pressure, u^s is the steady state pore water pressure and the soil elastic bulk modulus K is defined as follows:

$$K = \frac{E}{3(1-2\nu)} \quad (13)$$

By introducing u^e and u^s in the definition of the hydraulic head and by substituting ε_{vol} (Equation 12), Equation 11 can be rewritten as:

$$\frac{kK}{\gamma_w}\left(\frac{\partial^2 u^e}{\partial x_1^2} + \frac{\partial^2 u^e}{\partial x_2^2} + \frac{\partial^2 u^e}{\partial x_3^2}\right) = -\frac{\partial\, p}{\partial t} + \frac{\partial\, u^e}{\partial t} \quad (14)$$

By taking inspiration from the well-known one-dimensional consolidation theory, the following non-dimensional variables have been introduced:

- non-dimensional coordinates: $X_i = \frac{x_i}{D}$
- non-dimensional time: $T = \frac{t}{t_u}$
- non-dimensional excess pore water pressure: $U = \frac{u^e}{\sigma_{f0}}$
- non-dimensional total pressure: $P = \frac{p}{\sigma_{f0}}$

By introducing in Equation 14 all these non-dimensional variables it reads:

$$\left(\frac{\partial^2 U}{\partial X_1^2}+\frac{\partial^2 U}{\partial X_2^2}+\frac{\partial^2 U}{\partial X_3^2}\right)=-\Upsilon\left(\frac{\partial P}{\partial T}-\frac{\partial U}{\partial T}\right) \quad (15)$$

in which the non-dimensional excavation rate (Υ) is defined:

$$\Upsilon=\frac{\gamma_w D^2}{kKt_u}=\frac{3(1-2\nu)\gamma_w D^2}{kEt_u} \quad (16)$$

Equation 15 only depends on Υ. For this reason, once Υ is fixed the response of the system is unique (Appendix 4) at the local level (stresses and strain distributions) and at the global one (face characteristic curve, Equation 3).

Appendix 4

To demonstrate that, under partially drained conditions, once Υ is defined, the response in the Q_f-q_f plane is unique, the authors performed a series of analyses characterized by Υ=*20* and different D, k, E and t_u values (Table 3 and Figure 14). Boundary conditions and analyses phases are those employed for the analyses discussed in Section 2. The perfect coincidence of these curves is due to the value of the dilatancy employed (ψ=0°), which excludes any hydro-mechanical coupling associated with plastic strains. This also justifies the choice of employing, even if the soil behaviour is assumed to be elastic-perfectly plastic, the elastic properties in the definition of the non-dimensional excavation rate Υ (Equation 1).

Table 3: List of the parameters varied to obtain the numerical results of Figure 14 for H/D=5, γ_{sat}=20kN/m^3, v=0.3, ϕ'=25°, ψ=0° and k_0=1-sin ϕ'

	D [m]	E [MPa]	t_u [days]	k [m/s]
A	12	100	1	10^{-8}
B	12	100	10	10^{-9}
C	12	1000	1	10^{-9}
D	12	1000	0.1	10^{-8}
E	0.12	100	0.0001	10^{-8}

The local system response is analysed in terms of non-dimensional hydraulic head (h^*), defined as:

$$h^* = \frac{h-h_0}{h_0}, \tag{17}$$

where h is the current hydraulic head and h_0 is the initial value of h. For the sake of brevity, only the results corresponding Q_f=3 (point P of Figure 14) for analyses A and E (Table 3) are plotted in Figure 15 (for the sake of clarity, only a portion of the domain close to tunnel face is represented). The hydraulic head distributions in Figure 15a and 15b are practically coincident, suggesting that the local system response is unique for fixed ϒ and Q_f values.

The negative values of h^* close to the face and the positive values of h^* close to the lining clearly show that during the face unloading process, the water will flow toward the advance core. Moreover, the increase in pore pressure close to the lining, due to the stress migration from the advance core to the lining, confirms the stress redistribution taking place in the soil domain (also experimentally observed by Nomoto et al. 1999 and Berthoz et al. 2012a).

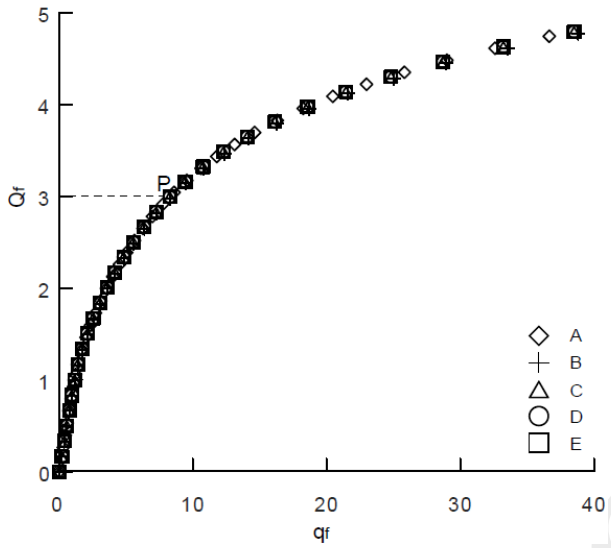

554

555 *Figure 14: Numerical results relative to ϒ=20 (Table 3)*

556

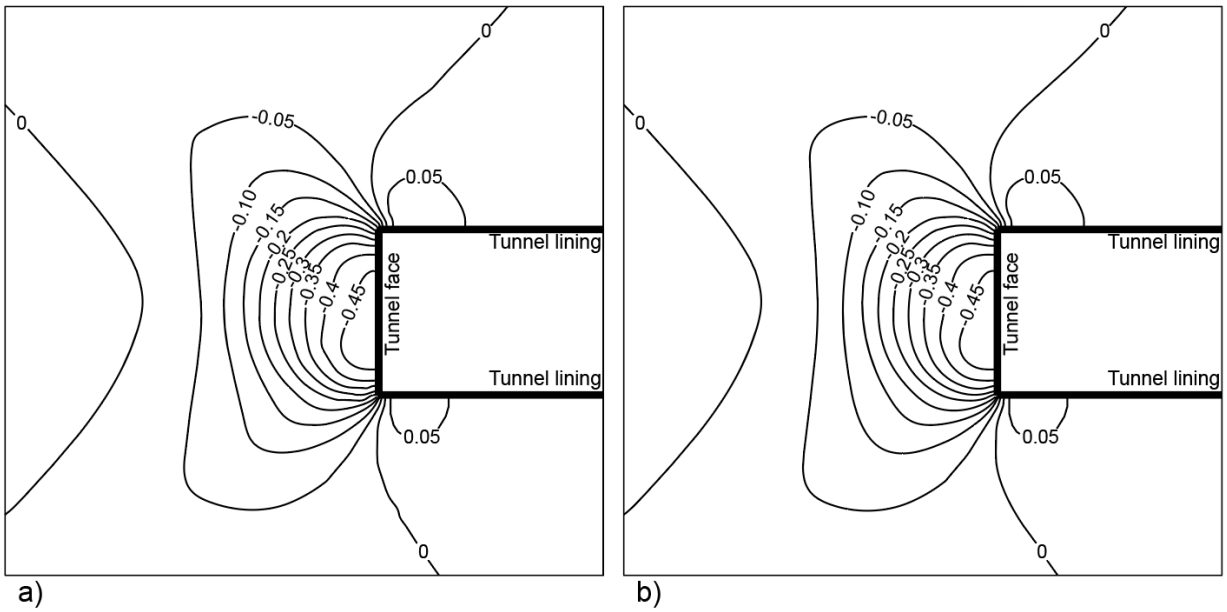

557

558 *Figure 15: Profiles of non-dimensional hydraulic head in the proximity of the face: a) analysis A of Table 3 (D=12m) and b)*
559 *analysis E of Table 3 (D=0.12m)*

560

561 **Appendix 5**

562 The expressions of functions $R(\Upsilon)$, $a_f(\Upsilon)$ and $Q_L(\Upsilon)$ of Equation 3, were derived from the

563 interpolation of numerical results (di Prisco et al., 2019b). In particular:

- $R(\Upsilon) = R_d + (R_u - R_d)\frac{0.065\Upsilon^{0.635}}{0.065\Upsilon^{0.635}+1}$, (18)

being R_u = 1 the non-dimensional undrained elastic stiffness, whereas R_d=0.725 is the corresponding drained stiffness. The numerical fitting is reported in Figure 16a.

- $a_f(\Upsilon) = a_{fd} + (a_{fu} - a_{fd})\frac{0.2\Upsilon^{0.635}}{0.2\Upsilon^{0.635}+1}$, (19)

being a_{fd}=0.686 the Q_f value for which yielding takes place under drained conditions, whereas a_{fu} is the corresponding undrained one. The numerical fitting is reported in Figure 16b. a_{fu}, as is shown in Figure 16c (adapted from di Prisco et al., 2018a), is not constant but a function of the initial (geostatic) total stress anisotropy factor $\bar{k}$ (i.e. the geostatic ratio of total horizontal and total vertical stresses).

- $Q_L(\Upsilon) = Q_{Ld} + 1.6\Upsilon$, (20)

where:

$$Q_{Ld} = \frac{\sigma'_{f0} - \sigma'_L}{s_u^*} \quad (21)$$

is the non-dimensional limit value of Q_f under drained conditions, σ'_{f0} the average effective horizontal geostatic stress applied on the tunnel face, whereas σ'_L is the minimum average effective pressure to be applied on the face to prevent its collapse under drained conditions, calculated according to Vermeer et al. (2003) as it follows:

$$\sigma_L' = (\gamma_{sat} - \gamma_w) D \left(\frac{1}{9 \tan \phi'} - 0.05 \right). \quad (22)$$

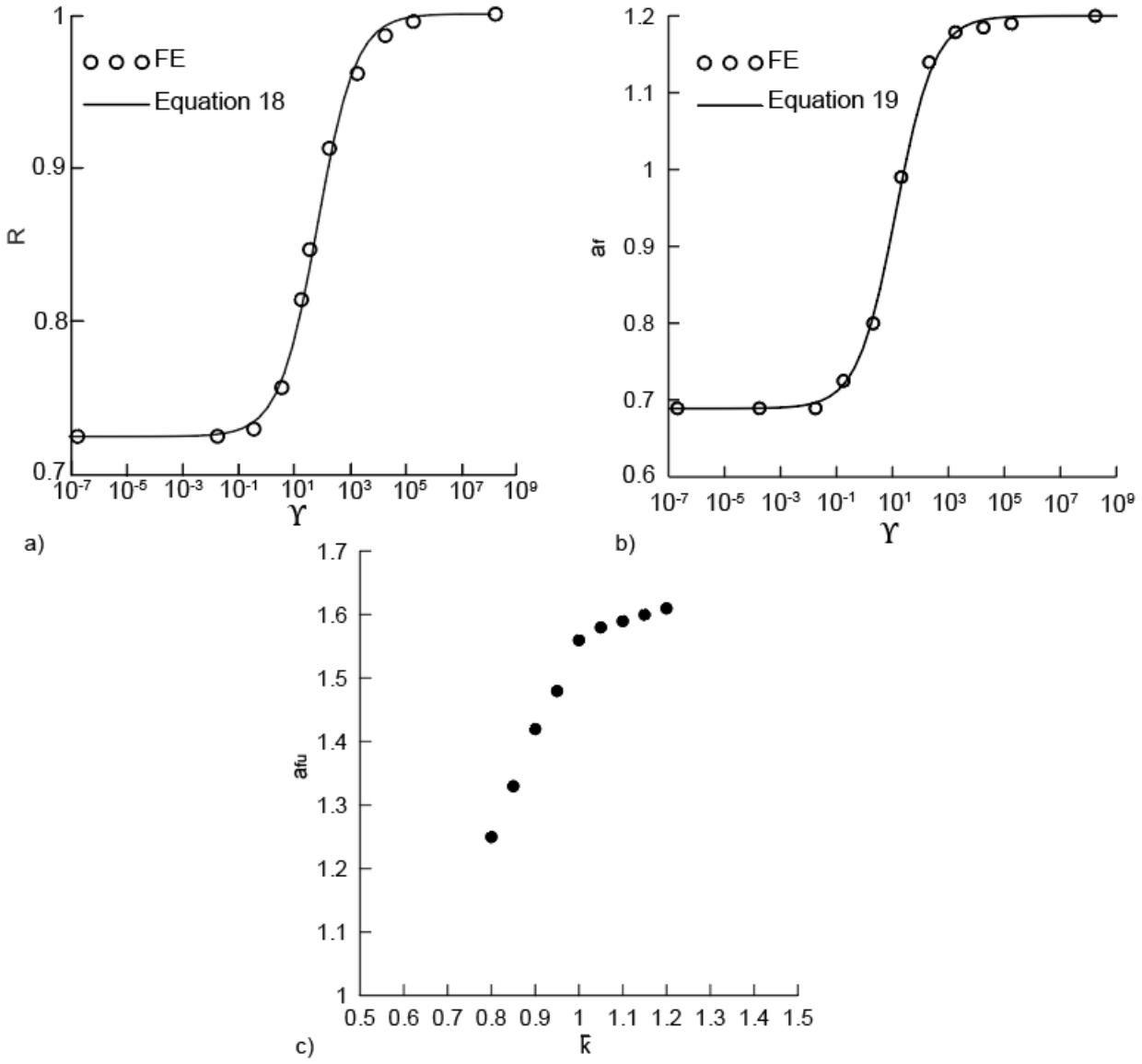

Figure 16. a) Variation of R with Υ, b) Variation of a_f with Υ c) Variation of a_{fu} with $\bar{k}$, adapted from di Prisco et al. (2018a)

References

1. Anagnostou, G. & Kovari, K. (1996), "Face stability conditions with earth-pressure-balanced shields," Tunnelling and Underground Space Technology, vol. 11, no. 2, pp. 165-173.

2. Attewell, P. & Farmer, I. (1974) "Ground disturbance caused by shield tunnelling in a stiff, overconsolidated clay," Engineering geology, vol. 8, no. 4, pp. 361-381.

3. Attewell, P. B., Yeates, J. & Selby, A. R. (1986), Soil movements induced by tunnelling and their effects on pipelines and structures, Blackie, Glasgow

4. Berthoz, N., Branque, D., Wong, H., Généreux, G., Subrin, D., & Humbert, E. 2012a. Tunneling in stratified soft ground: Experimental study on 1g EPBS reduced scale model. Geotechnical Aspects of Underground Construction in Soft Ground – Proceedings of the 7th International Symposium on Geotechnical Aspects of Underground Construction is Soft Ground 411-416.

5. Berthoz, N., Branque, D., Subrin, D., Wong, H., & Humbert, E. 2012b. Face failure in homogeneous and stratified soft ground: theoretical and experimental approaches on 1g EPBS reduced scale model. Tunnelling and Underground Space Technology, 30, 25-37.

6. Callari, C. (2004) "Coupled numerical analysis of strain localization induced by shallow tunnels in saturated soils," Computers and Geotechnics, vol. 31, no. 3, pp. 193-207, 2004.

7. Callari C. & Casini S. (2006), "Three-dimensional analysis of shallow tunnels in saturated soft ground," in Geotechnical Aspects of Underground Construction in Soft Ground - Fifth Int. Symp. TC28.

8. Callari, C. (2015) "Numerical assessment of tunnel face stability below the water table," in In: Proc. 14th IACMAG, 2007-2010, Kyoto., 2015.

9. Callari, C., Alsahly, A. & Meschke, G. (2017), "Assessment of stand-up time and advancement rate effects for tunnel faces below the water table," in 4th ECCOMAS Conf. on Computational Methods in Tunneling and Subsurface Engineering (EURO:TUN 2017), , Innsbruck

10. Chambon P. & Corté, J. F, (1994) "Shallow tunnels in cohesionless soil: stability of tunnel face," Journal of Geotechnical Engineering, vol. 120, no. 7, pp. 1148-1165

11. Chen, R. P., Li, J., Kong, L. G., & Tang, L. J. 2013. Experimental study on face instability of shield tunnel in sand. Tunnelling and Underground Space Technology, 33, 12-21.

12. Clough, G. & Schmidt, B., (1981) "The design and performance of excavations and tunnels," in Soft clay engineering, Developments in Geotechnical Engineering.

13. Cording E. & Hansmire W. (1975), "Displacements around soft ground tunnels," in 5th Pan American Congress on Soil Mechanics and Foundation Engineering, Buenos Aires.

14. Davis, E. H., Gunn, M. J., Mair, R. J. & Seneviratine H. N. (1980), "The stability of shallow tunnels and underground openings in cohesive material," Géotechnique, vol. 30, no. 4, pp. 397-416.

15. di Prisco C.; Boldini D.; Desideri A.; Bilotta E.; Russo G.; Callari C.; Flessati L.; Graziani A.; Meda A. (2022a) Computational methods In Handbook on Tunnels and Underground Works (pp. 203-245). CRC press.

16. di Prisco, C., Callari, C., Barbero, M., Bilotta, E., Russo, G., Boldini, D., ... & Sciotti, A. (2022b). Assessment of excavation-related hazards and design of mitigation measures. In Handbook on Tunnels and Underground Works (pp. 247-316). CRC press.

17. di Prisco, C., Flessati, L., Frigerio, G., & Lunardi, P. (2018a). A numerical exercise for the definition under undrained conditions of the deep tunnel front characteristic curve. Acta Geotechnica, 13(3), 635-649.

18. di Prisco, C., Flessati, L. Frigerio, G., Castellanza, R., Caruso, M., Galli, A., Lunardi, P. (2018b) Experimental investigation of the time-dependent response of unreinforced and reinforced tunnel faces in cohesive soils Acta Geotechnica: 13(3) 651-670

19. di Prisco, C., Flessati, L., Cassani, G., & Perlo, R. (2019a). "Influence of the fibreglass reinforcement stiffness on the mechanical response of deep tunnel fronts in cohesive soils under undrained conditions," in In Tunnels and Underground Cities: Engineering and Innovation meet Archaeology, Architecture and Art (pp. 1323-1331), CRC Press.

20. di Prisco, C., Flessati, L., Cassani, G., & Perlo, R. (2019b). Influence of the excavation rate on the mechanical response of deep tunnel fronts in cohesive soils. In Tunnels and Underground Cities: Engineering and Innovation meet Archaeology, Architecture and Art (pp. 3654-3663). CRC Press.

21. di Prisco, C., Flessati, L., Porta, D. (2020) Deep tunnel fronts in cohesive soils under undrained conditions: a displacement-based approach for the design of fibreglass reinforcements Acta Geotechnica, 15 (4), pp. 1013-1030. DOI: 10.1007/s11440-019-00840-8

22. Dimmock, P. S., & Mair, R. J. (2007). Estimating volume loss for open-face tunnels in London Clay. Proceedings of the Institution of Civil Engineers-Geotechnical Engineering, 160(1), 13-22..

23. Flessati & di Prisco (2022) A displacement-based approach for a face pressure assessment in mechanized tunnelling EURO:TUN 2021 5th International Conference on Computational Methods and Information Models in Tunneling Ruhr University Bochum, 22-24 June 2022

24. Flessati, L. & di Prisco, C. (2023) Deep tunnel faces in cohesive soils under undrained conditions: application of a new design approach, European Journal of Civil and Environmental Engineering, 27(8), pp 2630-2644 doi.org/10.1080/19648189.2020.1785332

25. Flessati, L. & di Prisco, C., (2018) "Numerical investigation on the influence of the excavation rate on the mechanical response of deep tunnel fronts in cohesive soils," in Springer series in geomechanics and geoengineering, pp 1140–1143., Wien

26. Flessati, L. (2017), Mechanical response of deep tunnel fronts in cohesive soils: experimental and numerical analyses, Ph.D. Thesis Politecnico di Milano.

27. Höfle, R., Fillibeck, J., Vogt, N. 2008 Time dependent deformations during tunnelling and stability of tunnel faces in fine-grained soils under groundwater. Acta Geotech 3, 309-316.

28. Höfle, R., Fillibeck, J., Vogt, N. 2009. Time depending stability of tunnel face. In: Proc. 35th ITA-AITES General Assembly, Budapest.

29. Horn, N. (1961) "Horizontaler erddruck auf senkrechte abschlussflächen von tunnelröhren.," in Landeskonferenz der ungarischen tiefbauindustrie.

30. Hu, X., Fang, Y., Walton, G., & He, C. (2022). Laboratory model test of slurry shield tunnelling in saturated sandy soil. Géotechnique, 73(10), 885-906.

31. Kamata, H., & Mashimo, H. 2003. Centrifuge model test of tunnel face reinforcement by bolting. Tunnelling and Underground Space Technology,18(2), 205-212.

32. Kimura, T. & Mair, R. (1981), "Centrifugal testing of model tunnels in soft clay. In Proceedings of the 10th international conference on soil mechanics and foundation engineering," in ISSMFE: International Society for Soil Mechanics and Foundation Engineering.

33. Kirsch, A. 2009. On the face stability of shallow tunnels in sand, PhD thesis Innsbruck University, Innsbruck.

34. Klar, A., Osman, S. & Bolton M., (2007) "2D and 3D upper bound solutions for tunnel excavation using 'elastic' flow fields," International journal for numerical and analytical methods in geomechanics, vol. 31, no. 12, pp. 1367-1374.

35. Kratz, B., Jehel, P., & Tatin, M. (2023). 3D numerical simulation of TBM excavation for predicting surface settlements-state of the art. Expanding Underground-Knowledge and Passion to Make a Positive Impact on the World, 2757-2765

36. Leca, E. & Dormieux L. (1990), "Upper and lower bound solutions for the face stability of shallow circular tunnels in frictional material," Géotechnique, vol. 40, no. 4, pp. 581-606.

37. Macklin, S. (1999) "The prediction of volume loss due to tunnelling in," Ground Engineering, vol. 32, no. 4, pp. 30-33.

38. Mair R. (1979), Centrifugal modelling of tunnel construction in soft clay, PhD thesis, Cambridge University.

39. Mair, R. & Taylor, R. (1997), "Theme lecture: bored tunnelling in the urban environment," in Proceedings of XIV ICSMFE, 1999.

40. Mitchell, R.J. (1983), Earth Structure Engineering, Allen and Unwin, Boston

41. Mollon, G., Dias, D. & Soubra, A. H. (2009), "Face stability analysis of circular tunnels driven by a pressurized shield.," Journal of geotechnical and geoenvironmental engineering, vol. 136, no. 1, pp. 215-229, 2009.

42. Mollon, G., Dias, D. & Soubra, A. H. (2013), "Continuous velocity fields for collapse and blowout of a pressurized tunnel face in purely cohesive soil," International Journal for Numerical and Analytical Methods in Geomechanics, vol. 37, no. 13, pp. 2061-2083.

43. Mühlhaus, H.B. (1985) "Lower bound solutions for circular tunnels in two and three dimensions," Rock Mechanics and Rock Engineering, vol. 18, no. 1, pp. 37-52.

44. Nomoto, T., Imamura, S., Hagiwara, T., Kusakabe, O., & Fujii, N. (1999). Shield tunnel construction in centrifuge. Journal of geotechnical and geoenvironmental engineering, 125(4), 289-300.

45. Peck, R. B. (1969). Deep excavations and tunneling in soft ground. Proc. 7th ICSMFE, 1969, 225-290.

46. Pferdekämper T. & Anagnostou G. (2022), "Undrained trapdoor and tunnel face stability revisited," Géotechnique Letters, vol. 12, no. 4, pp. 1-7.

47. Shang, W., Song, Z., Chen, Z., Chen, T., Meng, J., & Zheng, X. (2023). Experimental Investigation of Face Stability of a Slurry Shield Tunnel Based on a Newly Developed Model Test System. Geotechnical and Geological Engineering, 41(7), 4137-4152.

48. Sitarenios & Kavvadas, M. 2016. The interplay of face support pressure and soil permeability on face stability in EPB tunneling. In: Proc. WTC16, San Francisco.

49. Soe, T. E. E., & Ukritchon, B. (2023). Three-dimensional undrained face stability of circular tunnels in non-homogeneous and anisotropic clays. Computers and Geotechnics, 159, 105422.

50. Sterpi, D., & Cividini, A. 2004. A physical and numerical investigation on the stability of shallow tunnels in strain softening media. Rock Mechanics and Rock Engineering, 37(4), 277-298.

51. Vermeer, P. A., Ruse, N., & Marcher, T. (2002). Tunnel heading stability in drained ground. Felsbau, 20(6): 8-18.

52. Vu, M. N., Broere, W., & Bosch, J. (2016), "Volume loss in shallow tunnelling," Tunnelling and Underground Space Technology, pp. 77-90.

53. Wong, H. & Subrin, D. (2006) "Stabilité frontale d'un tunnel: Mécanisme 3D en forme de corne et influence de la profondeu," Revue européenne de génie civil, vol. 10, no. 4, pp. 429-456

List of Figures

List of Tables

List of symbols

a_f transition from linear to non-linear response in characteristic curves

a_{fd} drained value of a_f

a_{fu} undrained value of a_f

c' cohesion

D tunnel diameter

E soil elastic Young modulus

H tunnel cover

h hydraulic head

h* non-dimensional hydraulic head

h_0 initial hydraulic head

$i = k^* \left(H + \frac{D}{2}\right)$

K_{el} is a non-dimensional elastic parameter

K elastic bulk modulus

k permeability

k* amplitude of the gaussian settlement curve

$\overline{k}$ geostatic total stress anisotropy

k_0 at rest lateral earth pressure

778 L_a is the distance from the face from which stresses are practically not affected by the excavation

779 L_r lining segment length

780 $M_e = 6sin\phi'/(3 + sin\phi'))$

781 P non dimensional total pressure

782 p' and p are the effective and total pressure

783 p* geostatic effective pressure at tunnel axis depth

784 Q_f, q_f non-dimensional stress on the face and non-dimensional face extrusion

785 q_{adm} non-dimensional admissible displacement

786 Q_{fs}, q_{fs} supported Q_f and q_f

787 Q_{fus}, q_{fus} unsupported Q_f and q_f

788 Q_L limit value of Q_f

789 Q_{Ld} drained limit value of Q_f

790 R inclination of non-dimensional characteristic curves

791 S settlements

792 S_u* soil strength parameter

793 $S_{u,e}$ undrained strength under extension stress paths

794 t time

795 t_u time for excavate L_a

796 U non dimensional excess pore water pressure

797 u^e is the excess pore water pressure

798 u_f average face displacements

799 $u_{f,adm}$ admissible face extrusion

800 $u_{f,relu}$ the undrained elastic residual (i.e. for σ_f =0) face extrusion

801 u^s is the steady state pore water pressure

802 v_{ex} excavation rate

803 V_L volume loss

804 $V_{L,f}$ volume loss at the face

805 $V_{L,l}$ volume loss for long term effects

806 $V_{L,s}$ volume loss at the shield

807 $V_{L,t}$ volume loss at the tail

808 W_e volume of spoil associated with excavation rate

809 W_r ideal spoil volume

810 W_s spoil volume

811 x_1, x_2, x_3, X_1, X_2, X_3 dimensional and non dimensional coordinates

812 α strength parameter

813 δ average overcut

814 ε_{vol} volumetric strains

815 γ_{sat} soil saturated unit weight

816 γ_w water unit weight

817 ν Poisson ratio

818 σ_f average stress on the face

819 σ_{f0} geostatic average stress on the face

820 $\sigma_{f,TBM}$ is the pressure applied on the tunnel face by the TBM head

821 σ'_L limit effective pressure on the face

822 Υ non-dimensional excavation rate

823 ϕ' soil internal friction angle

824 ψ dilatancy